temperatures up to 7, 2, and 11 °K of the zero-pressure melting points of argon, krypton, and xenon, respectively.

As noted above, a true theory of melting must be based upon an equivalence of the Gibbs free energies of the solid and liquid. Nevertheless, within the context of our calculation the mechanical instability of our model correlated well (below 2 kbar) with the observed melting lines of solid argon, krypton, and xenon.

*Work supported by the U. S. Atomic Energy Commission.

[1]G. E. Jelinek, preceding paper, Phys. Rev. B 3 2716 (1971).

[2]M. Born and K. Huang, *The Dynamic Theory of Crystal Lattices* (Oxford U., New York, 1954).

[3]M. Born, J. Chem. Phys. 7, 591 (1939).

[4]F. D. Murnaghan, *Finite Deformations of an Elastic Solid* (Wiley, New York, 1951).

[5]F. Birch, J. Geophys. Res. 56, 227 (1952).

[6]J. J. Gilvarry, J. Appl. Phys. 28, 1253 (1957).

[7]O. L. Anderson, J. Phys. Chem. Solids 27, 547 (1966).

[8]J. R. MacDonald, Rev. Mod. Phys. 38, 669 (1966).

[9]J. W. Stewart (private communication); J. Phys. Chem. Solids 29, 641 (1968).

[10]J. R. Packard and C. A. Swenson, J. Phys. Chem. Solids 24, 1405 (1963).

[11]O. G. Peterson, D. N. Batchelder, and R. O. Simmons, Phys. Rev. 150, 703 (1966).

[12]A. C. Holt, W. G. Hoover, S. G. Gray, and D. R. Shortle, Physica 49, 61 (1970).

[13]K. F. Herzfeld and M. Goeppert-Mayer, Phys. Rev. 46, 995 (1934).

[14]J. DeBoer, Proc. Roy. Soc. (London) A215, 4 (1952).

[15]J. E. Lennard-Jones and A. F. Devonshire, Proc. Roy. Soc. (London) A170, 464 (1939).

[16]R. I. Kerber, J. Chem. Phys. 52, 2436 (1970).

[17]L. Hunter and S. Siegel, Phys. Rev. 61, 84 (1942).

[18]Y. Ida, Phys. Rev. 187, 951 (1969); Phys. Rev. B 1, 2488 (1970).

[19]P. H. Lahr and W. G. Eversole, J. Chem. Engr. Data, 7, 42 (1962).

[20]A. Michels and C. Prins, Physica 28, 101 (1962).

[21]J. C. Stryland, J. E. Crawford, and M. A. Mastoor, Can. J. Phys. 38, 1546 (1960).

[22]S. M. Stishov, I. N. Makarenko, V. A. Ivanov, and V. I. Fedosimov, Zh. Eksperim. i Teor. Fiz. 11, 22 (1970) [Sov. Phys. JETP Letters 11, 13 (1970).

[23]R. K. Crawford and W. B. Daniels, J. Chem. Phys. 50, 3171 (1969).

PHYSICAL REVIEW B VOLUME 3, NUMBER 8 15 APRIL 1971

Interference in LO-Phonon-Assisted Absorption*

Richard G. Stafford

Department of Physics, University of Oregon, Eugene, Oregon 97403

(Received 31 August 1970)

In this paper we calculate by second-order perturbation theory the optical absorption caused by the simultaneous creation of a Wannier exciton and a LO phonon. In insulators with $E_B \gg \hbar\omega_l$, a striking exhibition of quantum-mechanical interference is predicted for $\hbar\omega \approx E_{xn}$. Excepting for this interference effect, there are no sharp phonon peaks in the alkali halides if one assumes a linear exciton-phonon interaction. Peaks are predicted, but they are extremely broad and $\hbar\omega l$ can be placed energetically as a function of $\vec{K}$ anywhere in the Brillouin zone for $\hbar\omega > E_{xn} + \hbar\omega l$, by using presently available experimental and theoretical parameters.

I. INTRODUCTION

This paper presents an illustration of the quantum-mechanical interference effect found in excitonic transitions. The particular transition of interest is that of the absorption of a photon by an exciton with the simultaneous creation of an LO phonon. Since the process is a second-order one, the measurable effect in absorption is expected to be small and can, therefore, be said to be in the domain of fine structure. In conjunction with this, the effect has not previously been predicted, so that this may be a reason why it has not yet been reported as observed experimentally.

Segall[1] and Segall and Mahan[2] have considered the case for phonon-assisted emission, which is closely related to the absorption process. The threshold for emission is $E_{x1} - \hbar\omega_l$, whereas, for absorption, it is $E_{x1} + \hbar\omega_l$, which takes us into the thick of the exciton bands. For this reason, the excitonic intermediate states assume special importance in the following work. Another difference in approach is that their treatment was for semiconductors, where typically $E_B < \hbar\omega_l$. For our case, choosing $E_B \gg \hbar\omega_l$ facilitates a much cleaner theory to study the phonon effects. For this reason, we choose to apply our results to the alkali halides, and KI in particular, since E_B is less than the spin-orbit splitting, which again lends to a less complicated treatment. Another supporting feature of KI is the wealth of ex-

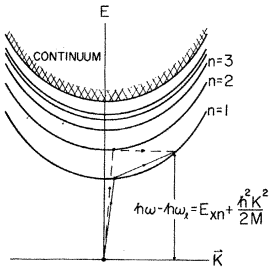

FIG. 1. Schematic of the simultaneous creation of an exciton and a phonon by the annihilation of a photon. The dot at $E=\vec{K}=0$ is the crystalline ground state (excitonic vacuum state). The parabolas represent the hydrogenic exciton bands, going from the discrete to the continuum.

perimentally determined parameters available for use in the calculations.

A last comment before getting to the calculations is that our treatment is for low temperature only, so that we can ignore phonon annihilation.

II. PHOTON ABSORPTION ASSISTED BY LO-PHONON CREATION

The calculation employs second-order perturbation theory using Fermi's Golden Rule. It can be easily pictured as in Fig. 1, where a vacuum-state exciton absorbs a photon of wave vector $\vec{k}$ and energy $\hbar\omega$ and makes a virtual transition to an intermediate excitonic state with $\vec{K}=\vec{k}$. The intermediate exciton then scatters into a final excitonic state with $\vec{K}=\vec{k}+\vec{q}\approx\vec{q}$ with the simultaneous creation of a phonon of wave vector $-\vec{q}$. Energy is conserved by the final state only, where the exciton has energy $E_x=\hbar\omega-\hbar\omega_l=E_{xm}+\hbar^2q^2/2M$ and the phonon $\hbar\omega_l$.

The transition probability from a vacuum-state exciton to a final-state exciton of energy $E_{xm}+\hbar^2K^2/2M$ and a phonon with energy $\hbar\omega_l$ and wave vector $-\vec{q}$ is given by

$$P_q^m(\hbar\omega)=\frac{2\pi}{\hbar}\left|\sum_n\frac{\langle G|H_{eR}|n,0\rangle\langle n,0|H_{eL}|m,K\rangle}{E_{xn}-\hbar\omega}\right|^2 \times\delta\left(\hbar\omega-\hbar\omega_l-E_{xm}-\frac{\hbar^2K^2}{2M}\right), \quad (1)$$

where H_{eR} is the electron-radiation interaction[3] and H_{eL} is the Fröhlich interaction[1,4] between the exciton and phonon. To obtain the absorption constant, we must sum over all $\vec{q}$:

$$\alpha^m(\hbar\omega)=\frac{nV}{Nc(2\pi)^3}\int d^3qP_q^m(\hbar\omega), \quad (2)$$

where n is the index of refraction, V is the volume of crystal, and N is the number of photons in V.

The similar process with phonon absorption has been previously evaluated by Segall and Mahan.[2] Their method is easily extended to cover phonon creation. The results of our calculations will be given in the terminology of the previous paper, and where there are basic differences in methods, these will be noted. Inserting $P_q^m(\hbar\omega)$ into $\alpha^m(\hbar\omega)$, we find

$$\alpha^m(\hbar\omega)=2\frac{E_{x1}^2\beta_1\alpha_p(\hbar\omega_l)^{3/2}}{nc|\phi_{1s}(0)|^2(2M)^{1/2}}\int d^3q\frac{1}{q^2} \times\left|\sum_n\frac{\phi_n(0)\langle n|U(q)|m\rangle}{E_{xn}-\hbar\omega}\right|^2\delta\left(\Delta_m-\frac{\hbar^2q^2}{2M}\right), \quad (3)$$

where

$$\Delta_m=\hbar\omega-\hbar\omega_l-E_{xm},$$

$$\langle n|U(q)|m\rangle=\int d^3r\phi_n^*(\vec{r})\left(e^{i\vec{Q}_e\cdot\vec{r}}-e^{i\vec{Q}_h\cdot\vec{r}}\right)\phi_m(\vec{r}).$$

The leading factor of 2 comes from spin degeneracy. The calculation of Ref. 2 incorrectly omits the term E_{x1}^2. Performing the integration over $\vec{q}$, the resulting expression is

$$\alpha^m(\hbar\omega)=\theta_m\xi\Delta_m^{-3/2}\left(\frac{\nu}{1-\nu}\right)^2\left|M_e^{-1}F_e^m-M_h^{-1}F_h^m\right|^2, \quad (4)$$

where

$$\xi=\frac{\pi E_{x1}^2\beta_1\alpha_p(\hbar\omega_l)^{3/2}\mu M}{nc\hbar B_1},$$

$$\theta_n=\begin{cases}1\\ \frac{1}{8}\end{cases}\quad\text{for } n=\begin{cases}1S\\ 2S\end{cases},$$

$$F_e^{1S}=\mathrm{Im}F[2,1;2-\nu;\tfrac{1}{2}(1-\nu+i\nu Q_e\alpha)],$$

$$F_e^{2S}=\mathrm{Im}\left(F[2,1;2-\nu;\tfrac{1}{2}(1-\tfrac{1}{2}\nu+i\nu Q_e\alpha)]-\frac{\nu}{2(2-\nu)}F[3,2;3-\nu;\tfrac{1}{2}(1-\tfrac{1}{2}\nu+i\nu Q_e a)]\right),$$

F is the hypergeometric function,

$$\nu_n=\left(\frac{B_1}{B_n-\hbar\omega_l-\Delta}\right)^{1/2},$$

B_n is the exciton binding energy for state n, and a is the exciton Bohr radius.

In the above, in addition to deriving the final $1S$-state absorption, the calculations have been extended to the $2S$ state. The major changes between absorption and emission of phonons can be most easily verified by referring to Refs. 1, 2, and 5.

These expressions will be evaluated in Sec. III. However, before doing so, an approximate expression for $\alpha^n(\hbar\omega)$ will be desirable to illustrate some of the principal points that will be discovered from the exact one. In addition to this, it will provide a check on the numerical evaluation of the exact expression, which is slightly beyond numeric intuition.

It will be sufficient to sum over the first three excitonic intermediate states to bring out the physics. The result is

$$\alpha'^{(m)}(\hbar\omega)\approx 2\eta\Delta_m^{-1/2}|\phi_{1S}(0)|^{-2}\left|\sum_{n=1}^{3}\frac{\phi_n(0)\langle n|U(q)|m\rangle}{E_{xn}-\hbar\omega}\right|^2, \quad (5)$$

where

$$\eta=2m^2B_1\xi/\mu M.$$

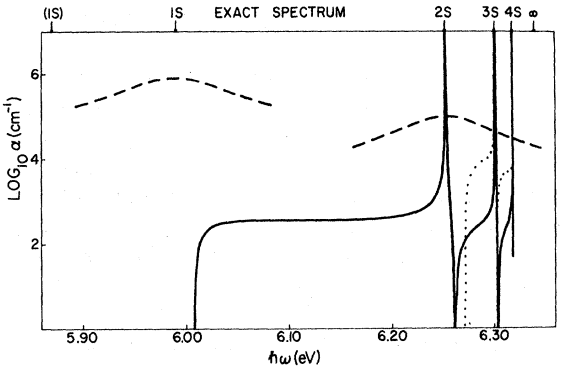

FIG. 2. Comparison of the Lorentzian zero-phonon and the exact LO-phonon-assisted absorption spectra. The dashed lines are the 1S and 2S Lorentzians; the solid line is the phonon assisted 1S, and the dotted line is the assisted 2S.

The term $\langle n|U(q)|m\rangle$ is easily evaluated, it being the difference of two Fourier transforms of the product $\phi_n^*(\vec{r})\phi_m(\vec{r})$.

III. RESULTS

For a quantitative comparison of results, a Lorentzian line shape is assumed for the one-photon absorption lines:

$$\alpha'^{(n)}(E) = 2\frac{\pi E_{x1}^2 \beta_1}{2nc\hbar}\left(\frac{\Gamma_n/2\pi}{(E-E_{xn})^2+\frac{1}{4}\Gamma_n^2}\right). \tag{6}$$

Using the constants in the Appendix, the one-photon and exact photon-phonon absorption spectra are compared in Fig. 2, while the approximation to the latter is plotted in Fig. 3.

These figures show that the phonon sidebands exhibit interference effects when $\hbar\omega \approx E_G - B_1/n^2$. The source of this is easily found in the approximate expression for α^n. A particular term like $\langle n|U(q)|m\rangle/(E_{xn}-\hbar\omega)$ varies most rapidly for $\hbar\omega \approx E_{xn}$ since $\langle n|U(q)|m\rangle$ is a slowly varying function of $\hbar\omega$. Therefore, the term goes through a sign change when $\hbar\omega$ crosses E_{xn}. Since the other terms of α^n are slowly varying in this region, they act like a continuum background. We must then have an interference minimum either above or below E_{xn}. Of course, the effect is most pronounced in the δ-function approximation. With acoustic-phonon broadening of the excitonic states, the interference shapes will also broaden, with both the peaks and depressions shifting in energy.

Considering the scale of Fig. 2, at first sight, only the peaks should exhibit a measurable contribution to the total α. On this, two points should be mentioned. The first is that the smallness of α^n should not be taken too seriously. By independently varying the hole effective mass between 0.398 and 10.0, it is possible to obtain a range in α^n from 0 to 10^6 cm^{-1}, thereby competing with the first-order process. Although this variation is artificial, it shows the sensitivity of α^n on M_h. For this reason, it would be desirable to have an experimental value for M_h, rather than to rely on its questionable derivation from other experimental parameters, as is done in the Appendix.

The second point is brought out by comparing α^{1S} and α^{2S}. Note that the latter is the larger. Although the other terms α^n for $n>2$ have not been considered here, they are not expected to change radically from the previous behavior. This behavior, coupled with the increasing density of states, may cause a large contribution to absorption by the phonon sidebands, independently of the above M_h effect.

If one adds these contributions to the zero-phonon spectra, very complicated fine structure can be constructed around the exciton resonances. This may contribute to an alternative explanation for some of the asymmetries and multifarious peaks seen in KI and other alkali halides.[6]

Comparing Figs. 2 and 3, one may note an order of magnitude discrepancy between the exact and approximate curves. Segall and Mahan[2] observe a similar type of behavior where the approximate expression gives a larger absorption than the exact one. Its origin here is explained by an increasing density of states,[1] as in the flat absorption shape of excitons in the vicinity of the bandgap.[3]

Toyozawa and Hermanson have stated that a second-order perturbation calculation of phonon-sideband shape predicts an absorption continuum starting at $E_{xn}+\hbar\omega_l$ and extending over a range of several $\hbar\omega_l$, with a peak occurring at $E_{xn}+(1+\nu)\hbar\omega_l$, where $\nu \approx 1$.[7]

The above statement is not borne out by our second-order calculation, except for the threshold condition. In fact, there is not peak in the sense given by them in the first Brillouin zone, when the exciton radius is of the same order as the lat-

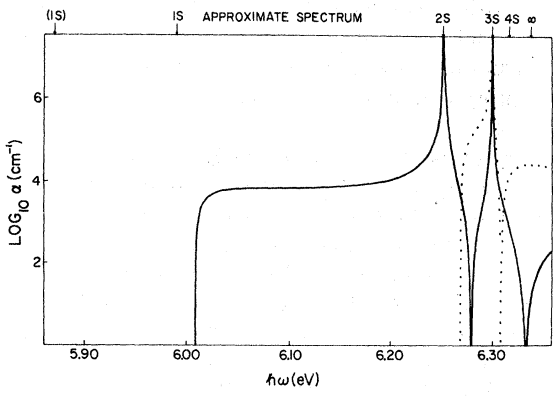

FIG. 3. Approximate LO-phonon-assisted absorption spectrum for the 1S and 2S final excitonic states.

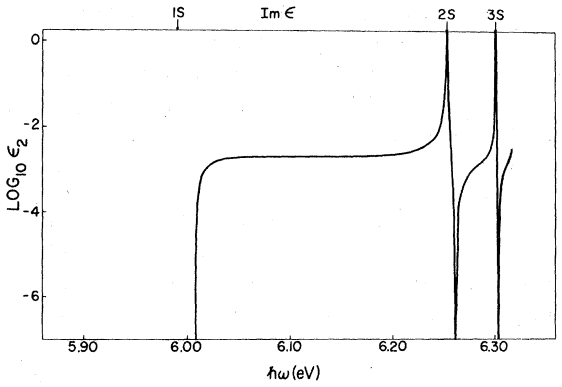

FIG. 4. Imaginary part of the complex dielectric constant.

tice parameter and ignoring phonon dispersion. Of course, exciton dispersion beyond the effective-mass approximation is not taken into account here. In the present case, the phonon sideband is extremely broad, extending over a large region of $\vec{K}$ space. This can easily be seen by again looking at the approximate expression for α^n. The key parameter is qa, which determines the basic behavior of $\langle n|U(q)|m\rangle$. To obtain a noticeable phonon-assisted peak within the first Brillouin zone, what is needed is to have the effective Bohr radius much greater than the lattice parameter. This changes qa, which determines where the Fourier transforms of $\phi_n^*\phi_m$ give structure such as peak position and width. A similar peak shifting can be accomplished by varying M_h, but the width remains extremely broad.

Wherever a phonon sideband peak may reside, within the present approximation, it most certainly can be found at energies greater than $\hbar\omega_l$, ignoring the exciton-phonon complex of Toyozawa and Hermanson[7] since their calculations are not valid for our case. In light of this, the recent statement made by Baldini *et al.*[6] to the effect that one cannot have phonon sideband peaks at energies greater than $\hbar\omega_l$, with linear exciton-phonon coupling, seems to contradict our results. With a proper choice of a, one can place a sideband peak anywhere one wishes, excepting within $\hbar\omega_l$ of the respective excitonic resonance.

Getting back to Figs. 2 and 3, it would be more accurate to consider the calculated absorption curves as being proportional to $n(\omega)\alpha(\omega)$, since n (ω) is a strong function of ω near resonance. A constant n was taken to facilitate the quantitative comparison of α^n with the experimentally known $\alpha'^{(n)}$.

A similar procedure can be used to obtain ϵ_2, which is better because it can be off by only a constant scaling factor rather than some wildly varying function of ω. We have $\epsilon_2 = (c/\omega)n\alpha = (c/\omega)A$, where $A = n\alpha \approx n'\alpha'$, and α' is the previously plotted (Fig. 2) absorption constant with typical approximate n'. ϵ_2 is given in Fig. 4.

It would be desirable to find ϵ_1 from ϵ_2 via Kramers-Kronig inversion, and thereby obtain the energy-loss function $-\mathrm{Im}\epsilon^{-1}$. However, a difficulty presents itself: The integral diverges in the δ-function approximation. This can be patched up by ascribing suitable half-widths and line shapes to the excitons. The only difficulty is that none of these are known with sufficient accuracy to obtain a meaningful expression for ϵ_1.

The interference effect predicted here has not yet been detected. The reflectivity experiment on KI of Baldini *et al.*[6] is the highest resolution work published to date, with a resolution of about 5 meV at 6 °K. Their results proved inconclusive regarding the observation of any interference effects. This is not surprising since the expected width of the interference dip is less than their resolution. What is needed is a resolution of about 0.1 meV. Since the effects of acoustic-phonon broadening are not accurately known, it might be worthwhile to perform the experiment at a lower temperature, perhaps around 1 °K.

As a final point, a comment is due on the similarity between the second-order–phonon-assisted absorption and the two-photon absorption processes. The symmetry between these two processes should lead us to expect a demonstration of interference in two-photon absorption. The previous methods can easily be extended to cover this situation and this should certainly be done. A case in point is the two-photon data of KI well into the band,[8] where a sharp decrease in absorption is seen for $\hbar\omega \approx E_{x1}$ on the low-energy side ($\hbar\omega_1$ is the probe beam). Interference is a probable explanation for this decline and this point will be actively pursued further later.

ACKNOWLEDGEMENTS

I should like to thank G. D. Mahan for suggesting this problem and for many valuable discussions while solving it. Thanks are also due to K. Park for his constant encouragement and suggestions.

APPENDIX: EXPERIMENTAL PARAMETERS USED IN CALCULATIONS

Table I presents the experimental parameters utilized in the calculations. These parameters represent a typical cross section of the literature and are not necessarily mutually consistent, there being serious problems in the alkali halides yet unsolved. It should be emphasized here that the energy for the 1*S* exciton was chosen to fit a hydrogenic series for calculational convenience in illustrating the interference effects. The actual location of the 1*S* state is lower as noted in the Table, and is accounted for by the central cell correction which

TABLE I. Experimental parameters used in calculations for KI.

E_G	6.34 eV[a]
E_B	0.35[a]
E_{x1}	5.99[a] (true = 5.87)[b]
$\hbar\omega_l$	0.018 (Ref. 6)
Γ_{1s}	0.1[a]
Γ_{2s}	0.087[a]
ϵ_∞	2.82 (b and Ref. 9)
ϵ_s	4.66[c]
M_e	0.398[c]
M_h	0.421
$\alpha'^{(1s)}$ (max)	8×10^5 cm^{-1} [d,e]

[a] J. J. Hopfield and J. M. Worlock, Phys. Rev. 137, A1455 (1965).

[b] J. Ramamurti and K. Teegarden, Phys. Rev. 145, 698 (1966).

[c] J. W. Hodby, J. A. Borders, and F. C. Brown, Phys. Rev. Letters 19, 952 (1967).

[d] H. R. Philipp and H. Ehrenreich, Phys. Rev. 131, 2016 (1963).

[e] K. Teegarden and G. Baldini, Phys. Rev. 155, 896 (1967).

no one has yet calculated. The true excitonic series for $n \geq 2$ is expected to fit the hydrogenic case fairly well. For a discussion of the problems involved in determining a proper value for the dielectric constant as seen by the exciton (see Ref. 9).

M_h is determined from the table by the following relation:

$$R^* = \mu^*/\epsilon^2\mu \text{ Ry}$$

or

$$M_h = M_e(RM_e/\epsilon^2\mu R^* - 1)^{-1},$$

where Ry is the hydrogenic Ry equal to 13.6 eV; $R^* = E_B$; μ is the hydrogen reduced mass; and μ^* is the exciton reduced effective mass.

The hole effective mass was determined from other parameters since there are neither experimental values nor reliable theoretical calculations for it. Since small variations in variables, such as the dielectric constant and binding energy have an appreciable effect on M_h, its use here should be construed as instructive only.

*Research supported in part by the National Science Foundation.

[1] B. Segall, Phys. Rev. 150, 734 (1966).

[2] B. Segall and G. D. Mahan, Phys. Rev. 171, 935 (1968).

[3] R. J. Elliott, Phys. Rev. 108, 1384 (1957).

[4] H. Fröhlich, Advan. Phys. 3, 325 (1954).

[5] L. Hostler, J. Math. Phys. 5, 591 (1964).

[6] G. Baldini, A. Bosacchi, and B. Bosacchi, Phys. Rev. Letters 23, 846 (1969).

[7] Y. Toyazawa and J. Hermanson, Phys. Rev. Letters 21, 1637 (1968).

[8] K. Park and R. G. Stafford, Phys. Rev. Letters 22, 1426 (1969).

[9] R. S. Knox, *Theory of Excitons* (Academic, New York, 1963).

PHYSICAL REVIEW B VOLUME 3, NUMBER 8 15 APRIL 1971

Lattice Vibrations in Deuterated Ammonium Chloride at 85° K. I. Experimental*

H. C. Teh and B. N. Brockhouse
Department of Physics, McMaster University, Hamilton, Ontario, Canada
(Received 23 July 1970)

Dispersion curves for the [00ζ] (Δ), [ζζ0] (Σ), [ζζζ] (Λ), and [$\frac{11}{22}$ζ] (*T*) directions in ND_4Cl were measured at 85 °K by inelastic scattering of slow neutrons using the McMaster triple-axis crystal spectrometer at Chalk River. The single crystals were grown from solution. A torsional (librational) branch, flat within about 2%, with an average frequency of 8.3×10^{12} cps, was found. Results are compared with a modified rigid-ion-model calculation based on Parlinski's formulation. Symmetry points and branches in the dispersion curves are classified according to their symmetry species. The Lyddane-Sachs-Teller relation as generalized by Cochran holds within experimental accuracy.

I. INTRODUCTION

In this paper the results of a study of the lattice vibrations in deuterated ammonium chloride ND_4Cl at 85 °K by inelastic scattering of neutrons are given. A preliminary report has appeared.[1] An accompanying paper by Cowley[2] gives additional theoretical analysis.

ND_4Cl has a cubic structure; the Cl^- ion is located at the corner and the tetrahedral ND_4^+ ion at the body center of the cube, with the hydrogen atoms at tetrahedral positions along the body diagonals. Thus the ND_4^+ ion is immersed in an electric field produced by the eight nearest Cl^- ions. There are two possible orientations of the ND_4^+ ion such that the hydrogens always point towards the nearest Cl^- ions. At room temperature the crystal is in a disordered phase in that the ND_4^+ ions are randomly